Modelling the spatial pattern of heatwaves in the city of Bern using a land use regression approach

Moritz Burger [a,b,*], Moritz Gubler [a,b,c], Andreas Heinimann [b,d], Stefan Brönnimann [a,b]

[a] *Oeschger Centre for Climate Change Research, University of Bern, Bern 3012, Switzerland*
[b] *Institute of Geography, University of Bern, Bern 3012, Switzerland*
[c] *Institute for Lower Secondary Education, Bern University of Teacher Education, Bern 3012, Switzerland*
[d] *Wyss Academy for Nature, Kochergasse 4, 3012 Bern, Switzerland*

ARTICLE INFO

ABSTRACT

Heatwaves have been the deadliest weather extreme events in Europe in the last decades. People living in cities are especially prone to such events due to the urban heat island (UHI) effect which increases the heat stress in urban surroundings especially during calm, steady, and radiation intensive synoptic situations. Since official measurement stations in cities are scarce, studies on spatial patterns of UHIs often rely on satellite data, hobby meteorologists' data, or on model outputs. Additionally, analyses of spatial UHI patterns using point-based measurements need adequate and cost-effective methods for spatial interpolation. In this study, air temperature data retrieved by 60 low cost measurement devices (LCD) are used to model the spatial pattern of the UHI with a land use regression (LUR) approach in Bern, Switzerland. For this purpose, 14 spatial variables with different buffer radii were calculated to evaluate their effect on the UHI and to interpolate the air temperature data. As a result, three models covering three different heatwaves at nighttime were developed. Given good model performance throughout the different scenarios, the here presented study demonstrates the successful interpolation of low cost temperature data by LUR modelling based on publicly accessible spatial information within a city.

1. Introduction

With ongoing anthropogenic climate change, longer, more intense, and more frequent heatwaves are expected worldwide (IPCC, 2014). Switzerland, situated at the borderline between the subtropical and temperate climate zones, is facing significant shifts with regard to summertime heat excesses in the future: Without drastic reductions in greenhouse gas emissions, daytime (e.g., increase of the hottest day of the year by 2–5.5 K) and nighttime temperature extremes (e.g., increase of tropical nights ($T_{min} \geq 20\,°C$) from 0–1 to 6–14) will increase markedly until the year 2060 (CH2018, 2018). Related negative impacts on human health make heatwaves the deadliest extreme weather events in Europe during the last decades (EEA, 2017), having caused an estimated additional death-toll in Switzerland of 1000 during the extreme summer of 2003 (Grize et al., 2005; Robine et al., 2007), 800 during the hot summer 2015 (BAFU, 2016) and 200 during the recent hot and dry summer of 2018 (BAFU, 2019). Following from this, the investigation of spatial and temporal patterns of heatwaves is crucial for the development and design of adaptation measures in order to minimize adverse

effects of heat on humans, the environment, and the economy.

Urban environments and their inhabitants are particularly prone to heat stress due to the well-studied "urban heat island (UHI) effect" (Stewart, 2011). It describes the phenomenon of air temperatures within a city being markedly higher when compared to its rural surroundings, especially during night (Stewart and Oke, 2012). Although different types of UHI related to different layers of the urban atmosphere exist (Oke, 1995), the canopy layer UHI, defined as the air temperature difference between the urban street canyon and the rural environment (Theeuwes et al., 2017), is most relevant for human health. The formation of a canopy layer UHI can be explained by the alterations of the urban energy balance: The construction materials used have a high heat capacity and thus store sensible heat during the day. In addition, those surfaces are usually dry or dry out quickly. In combination with a lack of vegetation and pervious surfaces, this leads to an enhancement of sensible heat fluxes, while latent heat fluxes are reduced (Oke et al., 2017). Furthermore, additional anthropogenic heat is released and stored in urban environments. Another important feature of the urban environment is an enhanced roughness layer, which is caused by the buildings and leads to a reduced mean airflow along with increased turbulence. In densely built urban areas, airflows in street canyons may even be completely separated from the flow above (Oke et al., 2017). In summary, these anthropogenic alterations lead to the situation that the emission of longwave radiation is obstructed and the loss of sensible heat much smaller in urban than in rural areas (Oke et al., 2017), which results in a typical diurnal evolution of the UHI, with maximum intensities during the evening and the night (Theeuwes et al., 2017). This diurnal cycle, however, varies depending on the weather conditions and the season (Morris et al., 2001). Besides the solar irradiance, the most important drivers of UHIs are windspeed and cloud cover, which in general lead to a weaker UHI magnitude (Morris et al., 2001). Therefore, an UHI is, at least in mid-latitude cities, ideally developed during summertime and situations with clear skies and low winds (Gehrig et al., 2018), which is a typical meteorological pattern for heatwaves. During such hot periods, health related risks are thus enhanced in urban areas due to the UHI (Köllner et al., 2017; Oke et al., 2017) and critical health-related thresholds can be reached due to the combination of generally high temperatures and additional urban heat, which highlights the importance of investigations on UHIs during heatwaves (Schatz and Kucharik, 2015). In view of continuously growing urban populations (UN, 2019) and demographic trends towards obsolescence (BFS, 2015) increasing the number of people at potential risk for severe heat stress (BAFU, 2016), research on the intensity and the local-scale variation of UHIs during heatwaves is strongly needed.

Over the last decades, the number of studies analyzing the UHI of cities has increased exponentially (Stewart, 2011; Deilami et al., 2018). If the canopy layer UHI is studied, the use of weather station data is recommended (Kato and Yamaguchi, 2007). However, official and automated measurement stations in urban environments are still scarce (Theeuwes et al., 2017) as well as expensive (Muller et al., 2013; Gubler et al., 2021). Some studies rely only on a single or a few measurement stations (e.g., Gehrig et al., 2018) which are classified as "rural" or "urban" stations. Due to the heterogeneity of microclimates in cities (Oke et al., 2017), the UHI effect is, however, a complex phenomenon which is only insufficiently described by a few single urban and rural sites (Stewart and Oke, 2012). In order to cope with the lack of urban measurement stations, past studies used data from hobby meteorologists (Steeneveld et al., 2011; Theeuwes et al., 2017), citizen weather stations (Meier et al., 2017), or mobile measurements (Ivajnšič et al., 2014). Nevertheless, the quality of such data is often limited by the spatial extent, the number of stations, or the accuracy of the sensors, and may be further affected by the temporal differences of mobile data (Chen et al., 2019). Another possibility is to use data retrieved by a purpose-designed measurement network consisting of numerous low cost temperature sensors and efficient radiation shielding. Networks of this kind have been installed in several cities such as Birmingham (Chapman et al., 2015), Tainan (Chen et al., 2019), or Bern (Gubler et al., 2021), of which the latter one is used to model UHI intensities in this study.

Since accurate estimations of the spatial variability of urban air temperatures are of interest for various stakeholders such as urban planners, city administrations, or energy suppliers, this raises the challenge of extrapolating UHI intensities from point-based measurements to the area of the entire city (Szymanowski and Kryza, 2009). One approach to face this challenge is to use land use regression (LUR) models. LUR modelling has been prominently used in air pollution studies, being interested in modelling small-scale variations within urban environments (Hoek et al., 2008). This geostatistical method combines data from monitoring stations with a set of predictor variables derived from different sources of spatial data, such as land use, topography, population density, or traffic volume (Hoek et al., 2008). Thereby, LUR models are capable to estimate the mean exposure level in areas without measurement stations (Shi et al., 2018), perform typically better or equivalent than other geo-statistical methods such as kriging (Hoek et al., 2008; Xie et al., 2011), have the potential of transferring models to other locations (Hoek et al., 2008), and are relatively cost efficient (Jerrett et al., 2005). The combination of LUR models with dense temperature measurement networks to investigate and map spatial patterns of UHIs is relatively new and has been used only in a small number of studies. Recently, a LUR modelling approach was applied to estimate the air temperatures using 43 spatial and temporal predictors in Hongkong (Shi et al., 2018). Based on the results of the LUR model, a spatial mapping of the UHI of Hongkong was done and an interpretation of the spatial variables discussed. However, the number of measurement stations was limited to a total of 42 (1 per 26 km^2) and a routine measurement network was used. One downside of such networks is that the investigators have no control over the selection and the variability of the monitoring sites (Hoek et al., 2008). Additionally, in this or similar studies, large areas with rather homogenous terrain were investigated (i.e., Zhou et al., 2014; Chen et al., 2019), which turns research on the ability of LUR-based UHI modelling in small or medium sized cities to be limited, which may be due to the assumption that heterogeneity of land use and topography within a study site is a possible limiting factor of LUR models (Jerrett et al., 2005).

This study aims to contribute to this research gap with the possibility of using air temperature data of a very dense urban network (1 per 1.5 km^2) and very precise and publicly available land cover and land use data. With that data the LUR modelling approach is tested in a setting of a rather small city with complex topography. It is thus a very different setting than the previously investigated cities. The aim of this study is to apply the LUR modelling approach to the city of Bern, Switzerland, during three heatwaves of the summers 2018 and 2019 using air temperature data from a network of 60 LCDs as well as 14 GIS (geographical information system) based predictor

variables. The performance of the LUR approach in estimating the spatial variability of UHI intensities in Bern, Switzerland is analyzed and discussed in order to prepare the ground for the design of adequate heat mitigation measures.

2. Materials and methods

2.1. Study area

The city of Bern is located in the central western part of the Swiss Plateau between the Alps and the Jura mountains on an average elevation of 550 m.a.s.l.. Its topography is complex and characterized by several hills (e.g., "Könizberg" (711 m.a.s.l.), "Gurten" (860 m.a.s.l.), and "Bantiger" (950 m.a.s.l.) as well as valleys such as the "Aaretal", "Köniztal", "Wangental", and "Worblental" (Mathys et al., 1980; Fig. 1). Additionally, the Aare river crosses the city of Bern on its way from the Alps to the Rhine and splits the city in a western and an eastern part. With 134′000 people living in the city and 400′000 inhabitants in its greater metropolitan area, Bern is the fifth largest city of Switzerland (BFS, 2019).
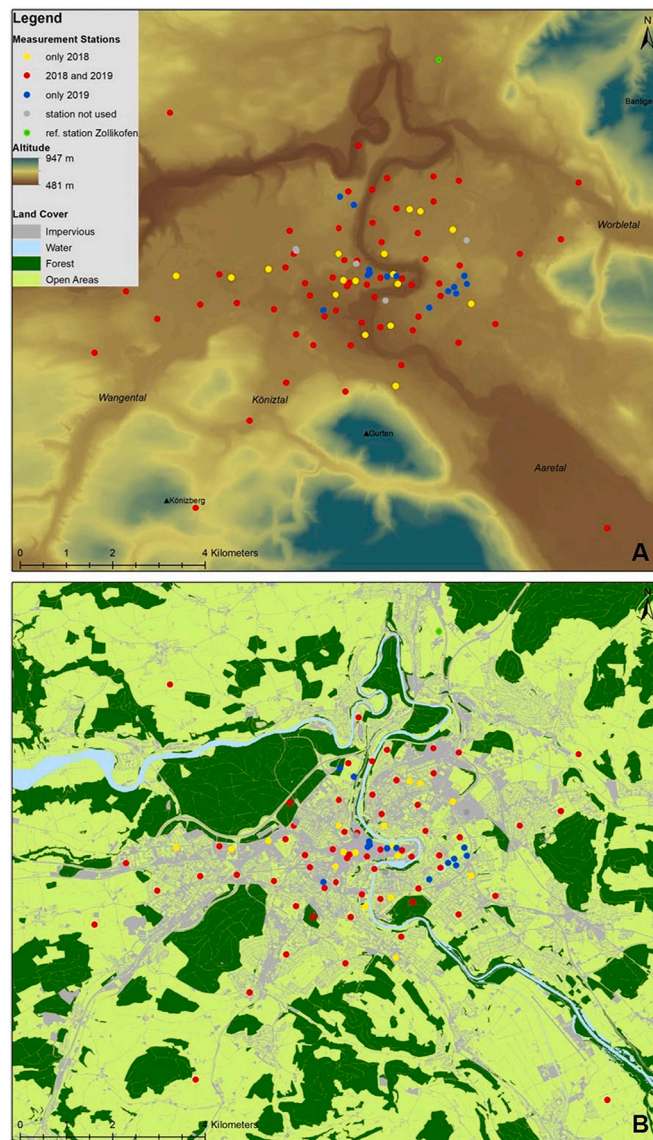

Fig. 1. Overview of the study area's topography (A) and land cover (B). Besides the most prominent topographic features, the measurement stations used in 2018 and 2019 are shown. Red dots show stations that were used in both years, yellow (2018) and blue (2019) dots mark stations that were only used during one measurement campaign, and grey dots show stations that were not used due to missing data or installation on incomparable elevations above ground (rooftops). (For interpretation of the references to colour in this figure legend, the reader is referred to the web version of this article.)

2.2. Climatology

2.2.1. General climatology of Bern

With an annual mean temperature of 8.8 °C and a yearly precipitation sum of 1059 mm (MeteoSwiss, 2018), Bern's climate zone, according to the Köppen-Geiger classification, is described as "warm temperature, fully humid, warm summer" (Kottek et al., 2006). In addition, summers are usually more humid than winters and reach daily mean maximum temperatures between 21.7 °C (June) and 24.3 °C (July). From 1981 to 2010, 6.3 hot days ($T_{max} \geq 30$ °C) were experienced per year on average, while tropical nights ($T_{min} \geq 20$ °C) did not occur during that period (MeteoSwiss, 2018). Due to the two mountain chains in the northwest (Jura) and the southeast (Alps), southwesterly and northeasterly flows dominate the regional wind dynamics (Wanner and Hertig, 1984). Additionally, in the city of Bern, weak southeasterly winds originating from the Alps and being canalized by the Aaretal (Fig. 1) are an important synoptic feature during nighttime (Mathys et al., 1980).

2.2.2. Climatology during the study period

Both summers investigated here (2018 and 2019) were exceptionally warm, reaching the fourth and the third rank in average summer temperature in Switzerland (MeteoSwiss, 2020). At the official measurement station in Bern-Zollikofen, overall mean summer temperatures were more than 2 K above the average summer temperatures and more than twice the amount of heat days were experienced (MeteoSwiss, 2018; Table 1). Additionally, both summers were rather dry, reaching only 76% (2018) and 84% (2019) of the long-term averaged summertime precipitation sums at Bern-Zollikofen (MeteoSwiss, 2019, 2020).

2.2.3. Heatwaves

Climate and temperature vary regionally, that is why no uniform definition of a heatwave exists (Meehl and Tebaldi, 2004). However, there is a need to work towards a unified framework for the definition of heatwaves which should not be too sector-specific and complex (Perkins, 2015). Commonly used metrics are the use of at least one form of temperature ("intensity") and a certain number of consecutive days ("duration"; Perkins, 2015). Thus, for this study, a rather simple, two-fold temperature threshold based on daily mean (T_{avg}) and maximum air temperature (T_{max}) was used. We defined heatwave by T_{max} and T_{avg} at Bern-Zollikofen being 5 K or more above the climatological mean summertime T_{max} and T_{avg} across the most recent reference period (1981–2010) for at least five consecutive days. Mean T_{max} and mean T_{avg} during summer (June–August) at the official measurement station in Bern-Zollikofen reached 22.3 °C and 17.3 °C (MeteoSwiss, 2018), hence the thresholds were defined at 27.3 °C and 22.3 °C (Fig. 2). Once a heatwave was detected, mean daytime (06:00–21:50) and nighttime (22:00–05:50) air temperatures were calculated.

Overall, three heatwaves were detected during summer 2018 and 2019: From July 30th to August 8th in 2018 (HW18), as well as from June 24th to July 1st (HW19.1) and July 20th to July 26th in 2019 (HW19.2; Fig. 2). Whereas mean T_{max} were almost equal during all heatwaves, mean T_{avg} show that HW19.1 was on average the most intense heatwave (Table 2).

2.3. LUR modelling

2.3.1. Temperature data from LCD measurement network

In order to measure the UHI variability of the city of Bern in detail, a dense network of low cost temperature measurement devices (LCDs) was installed during the summers of 2018 and 2019 (Gubler et al., 2021). Mounted on free-standing poles at 3 m above the ground, each sensor measured air temperatures every 10 min from mid-May to mid-September. In 2018, a total of 84 stations were installed, representing the heterogeneity of local climate zones, topographic characteristics, and gradients between rural, suburban, and urban surroundings of Bern (Fig. 1). In summer 2019, a total of 79 stations were installed. Some of the stations were displaced in comparison to 2018 due to a special focus on specific locations of interest. 64 sensors were placed at the same locations during both summers, whereof two stations had incomplete data during at least one heatwave and two stations were not installed at comparable elevations above ground (rooftops). For the LUR models, the remaining 60 stations with full data records throughout both summers have been used.

In order to assess the quality of the LCD temperature data, inter-comparisons between three LCDs and automated weather stations in three reference sites in different environments (urban, suburban, and rural) were conducted in summer 2018 (Gubler et al., 2021). A mean positive bias of 0.61 to 0.93 K (RMSE: 0.78 to 1.17 K) during daytime and eventually negative biases of −0.12 to 0.23 K (RMSE: 0.19 to 0.34 K) during nighttime were identified when averaged over the entire study period. During the heatwave 2018, hourly averaged biases were larger during daytime (0.7 to 2.2 K), but still relatively small during nighttime (−0.5 to 0.5 K: Gubler et al.,

Table 1
Mean summer temperatures (T_{avg}) and experienced hot days (HD) at the official measurement station at Bern-Zollikofen during the norm period (1981–2010), and during 2018 and 2019.

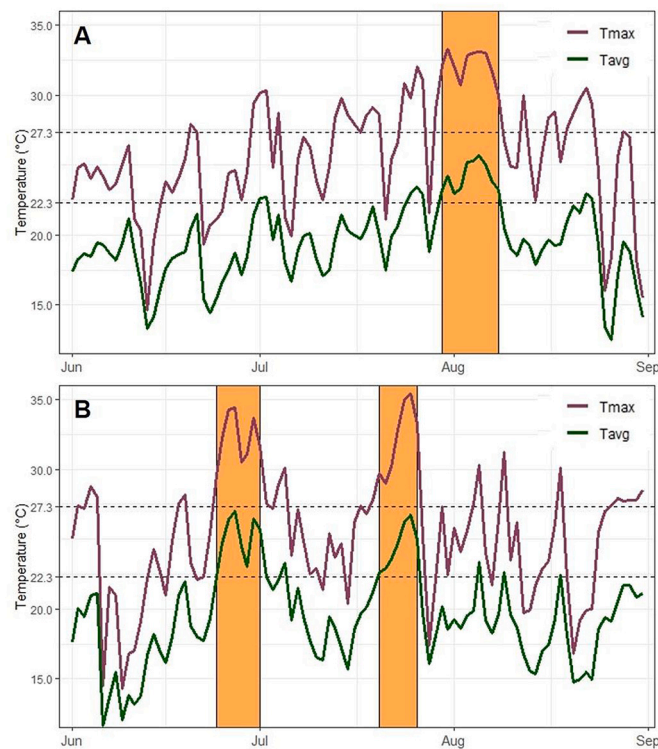| Period	Norm		2018		2019	
	T_{avg}	HD	T_{avg}	HD	T_{avg}	HD
June	16.0 °C	0.9	18.0 °C	0	19.0 °C	6
July	18.3 °C	3.0	20.4 °C	7	20.6 °C	7
August	17.7 °C	2.2	20.3 °C	10	18.8 °C	3
Entire summer	17.3 °C	6.1	19.6 °C	17	19.5 °C	16

Fig. 2. Daily maximum temperature (purple) and daily mean temperature (green) during summer 2018 (A) and 2019 (B) at the official measurement station at Bern-Zollikofen. Dashed lines mark the thresholds for heatwaves, whereas orange sections mark the heatwave periods. (For interpretation of the references to colour in this figure legend, the reader is referred to the web version of this article.)

Table 2
Duration (Days), mean maximum temperature (T_{max}) and mean average temperature (T_{avg}) of the observed heatwaves.

Heatwave	Duration (Days)	Mean T_{max}	Mean T_{avg}
HW18	10	32.17 °C	24.18 °C
HW19.1	8	32.18 °C	25.02 °C
HW19.2	7	32.19 °C	24.52 °C

2021). Most of the differences during daytime were attributed statistically to insufficient ventilation and radiative heating (Gubler et al., 2021).

Since the development of a canopy layer UHI is mainly a nighttime phenomenon (Oke et al., 2017) and the biases of the LCDs were much larger during the day than during the night (Gubler et al., 2021), the focus of this study lies on the nighttime situation. However, daytime LUR models and UHI maps were also conducted (see supplementary material for corresponding models, maps, and discussion of these).

2.3.2. Response variable: UHI intensity

The official, WMO-certified weather station of the city of Bern is located in a rural surrounding (Zollikofen), about 5 km north of the city center. It is operated by the Swiss Federal Office of Meteorology and Climatology (MeteoSwiss; Fig. 1). One LCD was installed next to the station of MeteoSwiss, at 3 m above ground. This station was used as rural reference to derive urban-rural temperature differences. Hence, we defined the UHI intensity as the difference in air temperature between any station of the measurement network and the LCD situated in Zollikofen. Since the height above sea level was not used as a criterion to choose the LCD locations, we incorporated the influence of the altitude directly with a dry-adiabatic decrease of 1 K per 100 m (Salvato et al., 2003), which was chosen since heatwave periods with a rather dry atmosphere were analyzed. This altitude corrected temperature (to the height of Bern-Zollikofen, 553 m.a.s.l.) is further referred as corrected temperature. The mean UHI intensity per heatwave was then used as the response variable in the three resulting models.

2.3.3. Predictor variables

To estimate UHI intensities for the entire urban area of Bern, a set of 14 spatial predictor variables was derived from publicly

available land use and land cover data. The selection of the variables was conducted based on their potential contribution to local air temperatures found in previous studies (i.e., Shi et al., 2018) and with regard to data existence in whole Switzerland in order to enable possible future transferability of the models (Hoek et al., 2008). The variables were grouped into four different functional categories: Land cover, topography, vegetation, and urban surface geometry (Table 3). For each variable, different circular zones around each measurement site ("buffer zones") were tested in order to investigate the spatial variability of the variables at different distances from the measurement location (see 2.3.4). The predictor variables are subsequently briefly described. All variables were extracted and calculated with the Software ArcGIS, Version 10.4 (ESRI, 2016) and QGIS, Version 3.4 (QGIS Development Team, 2018).

2.3.3.1. Land cover. For this category, data from the yearly updated official cadastral survey of the Canton of Bern was used (AVR, 2019). The 25 land cover surface categories in the original dataset were reclassified into 6 categories: These categories are "land cover buildings" [LC_B], "open space sealed" [OS_SE], "open space water" [OS_WA], "open space forest" [OS_FO], "open space agriculture" [OS_AC] and "open space garden" [OS_GA]. Within one buffer, all land cover variables were summed up to a value of 1 with different categories represented by the relative share in percent.

2.3.3.2. Topography. This group of variables contains potential contributing factors with regard to the natural topography. Elevation was derived from a high-precision digital elevation model (DEM) of swisstopo (swissALTI³ᴰ) from the year 2018, which contains precise elevation information in a 2×2 m raster file. This data was used to calculate the variables "slope" [SLO], "northness" [NOR] and "flow accumulation" [FLAC]. The variable "slope" was defined with the average elevation gradient in degree [0–90] of the DEM. The variable "northness" was calculated according to Ivajnšič et al. (2014) with the cosine of the aspect of the landscape. Values close to 1 describe a northern exposition, values close to −1 a southern exposition and values close to 0 a western or eastern exposition. The variable "flow accumulation" was calculated with the geoprocessing tools "flow direction" and "flow accumulation" in ArcGIS. These tools calculate the flow of a cell to its neighboring downslope cell (flow direction) and accumulate all their flows and the accumulated weight in a raster file (ESRI, 2016). This technique is widely used in hydrology to model the flow of water over a surface (Bigg et al., 2014). Since cold air drainage is driven by gravity in a similar way than water (Bigg et al., 2014), the variable may also be used as a proxy for cold air flow and accumulation in topographic complex regions (Chung et al., 2006). Hence, the variable FLAC was here used as a proxy for cold air flows originating from the hills around Bern.

2.3.3.3. Vegetation. Vegetation properties are key variables for UHI intensities, since evapotranspiration is one of the most important factors for surface air temperature (Köllner et al., 2017). Locations of the single trees were gained from a topographic landscape model (swissTLM³ᴰ) provided by swisstopo. Unfortunately, there is no information about the exact number of trees across forests. For this reason, the tree density in forests was estimated by assuming 0.02 trees per m², which is a rather low number for temperate forests (Crowther et al., 2015) but approximately corresponds to the number of tall trees, which was estimated by site inspections at the forests of Bern. The number of trees within a certain buffer results in the variable "amount of trees" [AMT].

The second variable used with regard to vegetation is vegetation height. A canopy height model with a resolution of 0.5 m for Switzerland was received from the Swiss Federal Research Institute WSL, which was calculated with data from swisstopo (swissALTI³ᴰ and swissTLM³ᴰ; see Ginzler and Hobi, 2015). For this study, the data was resampled to a 5×5 m grid whereas the mean value within a certain buffer resulted in the variable "vegetation height" [VH].

2.3.3.4. Urban surface geometry. In this fourth category, key properties of urban features are included in the model. Detailed information about the location and height of the buildings were derived from another swisstopo dataset (swissBUILDINGS³ᴰ2.0). The average height of the buildings within a certain buffer returned the first variable on urban surface geometry: "mean building height" [MBH]. The second variable "building volume density" [BVD] was calculated using the same data set. The measurement station with

Table 3
The 14 spatial variables used in this study with its abbreviation, its buffer radii tested, its units and its chosen buffer radii during nighttime.

Category	Variable	Abbreviation	Buffer radii tested	Unit	Chosen buffer radius (m)
Land cover	Land cover buildings	LC_B	25/50/150/250/500	%	250
	Open space sealed	OS_SE	25/50/150/250/500	%	500
	Open space forest	OS_FO	25/50/150/250/500	%	250
	Open space garden	OS_GA	25/50/150/250/500	%	25
	Open space water	OS_WA	25/50/150/250/500	%	150
	Open space agriculture	OS_AC	25/50/150/250/500	%	500
Topo-graphy	Slope	SLO	24_25/50/100 150_150/500	°	24_100
	Northness	NOR	50/150	−1 to +1	150
	Flow accumulation	FLAC	24_50/100/150/200 150_150/250/500		150_200
Vegetation	Amount of trees	AMT	25/50/100	nmbr.	100
	Vegetation height	VH	25/50/100/150/200	m	150
Urban surface geometry	Mean building height	MBH	25/50/100/150/200	m	150
	Building volume density	BVD	25/50/100/150/200	0 to 1	200
	Sky view factor	SVF	25	0 to 1	25

the largest BVD (height x ground cover) within a certain buffer was then rescaled such that the station with the largest BVD receives a maximum of 1.

The third variable of this category is the "sky view factor" [SVF]. The sky view factor describes the visible fraction of the sky at a certain point in the street canyon (Theeuwes et al., 2014) and is summarized in a number between 1 (sky totally visible) to 0 (absolutely no sky visible). It was calculated with the UMEP package in QGIS, which uses a digital surface model and a tree coverage model (Lindberg et al., 2018). The digital surface model was derived by a combination of swissALTI³D and swissBUILDINGS³D2.0, the tree coverage model with the vegetation height layer of the WSL. For the transmissivity of the tree layer, an average value of 3% was used (Konarska et al., 2014).

2.3.4. Buffer zone radii

Buffer zones are circular areas around the measurement stations. Since the impact of different variables on the local energy balance varies by distance (Shi et al., 2018), the selection of adequate buffer zone radii is crucial for the performance of the model (Hoek et al., 2008). Within a certain buffer zone, the mean or the sum of the variable was conducted. Different buffer zone radii were tested for each variable ranging from 25 to 500 m (Table 3). For the variables of the group "topography", different resolutions of the DEM with different buffer radii were additionally tested. Critical buffer selection from previous LUR studies (Zhou et al., 2014; Shi et al., 2018) were used as indicators for the buffer radii to be evaluated.

The evaluation of buffer radii was conducted by linear regression modelling. For every heatwave detected, the mean UHI intensities during daytime (see supplementary material) and nighttime were used as the dependent variables. Each buffer radius was then linearly fitted with the dependent variable. The resulting amount of explained variance (R^2) value was taken as the indicator for the strength of the model. The buffer radius with the highest R^2 was then chosen for the LUR model (Table 3). If the results differed between the heatwaves, a decision for the most logical buffer radius was made.

2.4. Statistical modelling and validation

Multilinear regression LUR modelling was conducted using the 14 spatial variables within the specific buffer radii to robustly predict day- and nighttime UHI intensities during all heatwaves. A hybrid version of forward and backward stepwise selection was performed with the statistical software R (R Development Core Team, 2008) in order to maximize the adjusted coefficient of determination (R^2_{adj}). Further, we excluded variables during the selection process which showed no significance ($p > 0.1$ during more than one heatwave), or which did not show a similar level of significance or the same sign during all heatwaves. This approach combines the computational advantages of forward and backward selection (James et al., 2013) without losing the control to purely statistical methods. The resulting multilinear regression equations were then used to calculate the UHI intensity maps at a resolution of 50×50 m in ArcGIS.

Validation of the LUR models is crucial for the evaluation of their performance and for model intercomparisons (Hoek et al., 2008).
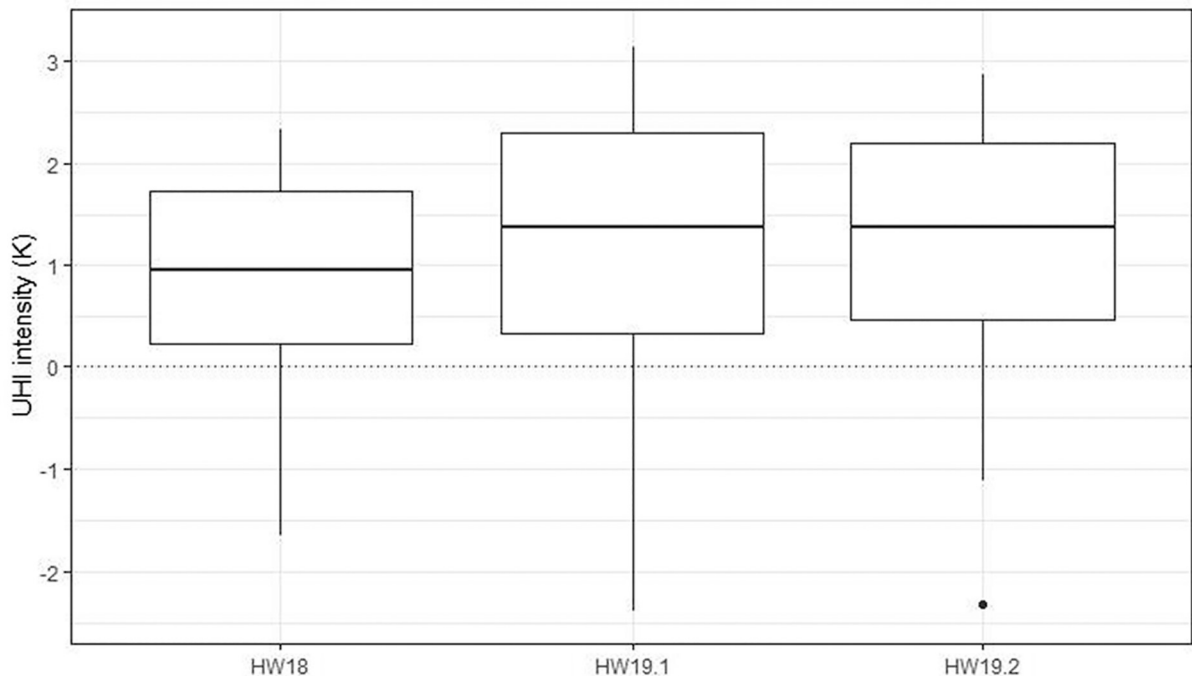

Fig. 3. Boxplots of nighttime UHI intensities (corrected air temperatures) of the 59 measurement stations during the three heatwaves.

Leave-one-out cross validation (LOOCV) as well as sub-dividing the monitoring sites in a training and a validation set (Validation Set Approach; see James et al., 2013) are methods that are often used in LUR studies (Hoek et al., 2008). In this study, both validation methods were conducted in order to compare the root mean square errors (RMSE) of the data and to check the validity of the models. The validation set approach was conducted using data of the additional measurement stations that have been operated solely in 2018 and 2019 (Fig. 1).

3. Results

In the following, we focus on the results of the nighttime models due to the UHI being a predominantly nocturnal phenomenon and the uncertainty arising from potential radiative biases in the measurement data (Gubler et al., 2021). For the matter of transparency, however, daytime models and resulting UHI maps including a brief discussion of it can be found in the supplementary material.

3.1. Mean differences in corrected air temperature compared to Bern-Zollikofen

The median nighttime differences of the 59 LCDs during the heatwaves vary between 0.9 and 1.4 K (Fig. 3), meaning that the majority of measurement locations measured higher temperatures than the rural reference and that the differences during the night were larger than during the day (0.3 to 0.9 K; see supplementary material). During all three heatwaves, however, negative median UHI intensities of up to −2.5 K indicate that some stations are being situated in considerably cooler environments than the rural reference station in Bern-Zollikofen. When intercomparing the heatwaves, HW18 shows a lower positive median value as well as reduced positive extremes than the two heatwaves in 2019. Positive and negative extremes are most pronounced during HW19.1 with a spread of more than 5 K in average corrected nighttime temperatures (Fig. 3).

3.2. LUR models

A total of three models were developed, one for each heatwave (Table 4). The R^2 score is the highest during HW18 (0.8) and slightly lower during HW19.2 (0.77) while the *p*-values are below 0.0001 for every heatwave (Table 4). Variables from land cover, topography, and vegetation categories were selected, whereas no variable from urban surface geometry was significant. The six variables are equally divided in three warming (positive sign: LC_B, OS_SE, VH) and three cooling factors (negative sign: OS_WA, FLAC, AMT). The regression coefficients of all variables increase from HW18 to HW19.1, but the rate of the increase varies. Nighttime error prediction plots (Fig. 4) show that the errors of single stations were largest during HW19.1 and smallest during HW18. Additionally, the plots indicate that during all heatwaves, the stations with the largest positive UHI intensities were rather slightly overestimated (ca. 0.1 to 0.5 K; see Fig. 4).

The RMSEs of the models increase from HW18 to HW19.1 (Table 5). Model validation shows that LOOCV RMSEs are relatively close to the model RMSE with differences smaller than 0.1 K (Table 5). When compared to additional stations data, RMSEs increase in all models, but much stronger at the models of 2019 than at the HW18 model. Comparisons of the LOOCV and the additional data RMSE show the same pattern than the model RMSE, with errors being the smallest at HW18, medium at HW19.2 and largest at HW19.1.

3.3. Spatial UHI variability during heatwaves based on LUR models

Detailed nocturnal UHI maps with a resolution of 50 × 50 m were calculated based on the LUR models. Nighttime maps show maximum UHI intensities between 3 and 4.5 K depending on the heatwave, with the highest values being reached during HW19.1 (Fig. 5). During the day, the modelled UHI intensities are much weaker, with maxima of up to 2 K (supplementary material). The spatial distribution of the nighttime UHI is markedly affected by the Aare river which acts as a cooling stream within the warm city. The cooling effect of the river seems strongest during HW19.1 (Fig. 5B) and weakest during HW18 (Fig. 5A). Additionally, cold air accumulations seem to be an important feature during all three heatwaves with strong cooling effects in the valleys "Köniztal" in the south and "Worblental" in the northeast. Due to the cooling barrier induced by the river, two distinct UHI hotspots can be observed: One at the upper old town in the city center with the highest values and another in the east of the city at the industrial zone "Galgenfeld" with only slightly lower values. Besides the river and the zones of cold air accumulation, forests and city parks create cool spots within the city with a cooling between 0.5 K (small parks) and 2 K (larger city parks or forest).

The differences between the measured and the modelled values indicate that our model has a negative bias in the eastern part and a slightly positive bias at the western part of the city (Fig. 6), which means that the eastern part was modelled too cold and the western part too warm. The same pattern is also observed during daytime (supplementary material). Furthermore, corrected temperatures

Table 4
Resulting nighttime model structure and model performance during the three heatwaves.

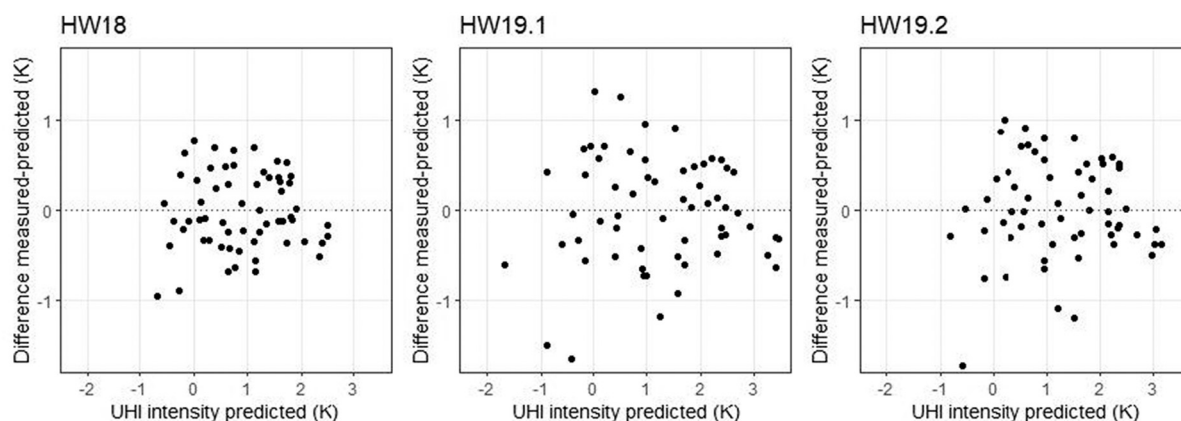| Heatwave	Model structure	Model performance		
		R^2	R^2_{adj}	*p*-value
HW18	3.332 (LC_B) + 2.986 (OS_SE) + 0.046 (VH) - 2.670 (OS_WA) - 0.018 (FLAC) - 0.005 (AMT) - 0.149	0.7988	0.7761	<0.0001
HW19.1	5.132 (LC_B) + 3.737 (OS_SE) + 0.114 (VH) - 7.984 (OS_WA) - 0.023 (FLAC) - 0.008 (AMT) - 0.242	0.7964	0.7734	<0.0001
HW19.2	4.005 (LC_B) + 3.619 (OS_SE) + 0.088 (VH) - 5.120 (OS_WA) - 0.020 (FLAC) - 0.007 (AMT) - 0.037	0.772	0.7462	<0.0001

Fig. 4. Predicted (x-axis) versus the difference of measured-predicted nocturnal UHI intensities (y-axis) of the 60 measurement stations.

Table 5
Resulting RMSEs of the model output, the LOOCV cross validation and the validation with the additional data of the stations not used in the models during the three heatwaves.

Heatwave	Model RMSE	LOOCV RMSE	additional data RMSE
HW18	0.4221 K	0.4716 K	0.5016 K
HW19.1	0.6150 K	0.7014 K	0.9450 K
HW19.2	0.5451 K	0.6210 K	0.7825 K

close to the Aare river are rather modelled too warm. The largest errors are found at the rural stations outside of the city. Whereas the stations in the southeast and in the west show a positive bias larger than 1 K, the station located in the Köniztal in the south shows a negative bias exceeding −1 K. However, the errors of the rural stations north and east of the city were rather small. The spatial patterns of the errors are similar during all three heatwaves.

4. Discussion

4.1. Applicability of the LUR model approach for the city of Bern

4.1.1. Performance of LUR models

Overall, the performance of the LUR models for estimating nighttime UHI intensities in Bern is in the same range than that reported in previous UHI linear regression modelling approaches (Shi et al., 2018; Gehrig et al., 2018; Chen et al., 2019), although comparability is limited as the setting in these studies (i.e., number of measurement stations, used spatial predictors, complexity of the study site) differs from ours. One explanation for the good performance of our models may be the focus on rather short heatwave periods. Since heatwaves in mid-latitudes are usually caused by stable high pressure anticyclones associated with low winds as well as dry and radiation intensive weather (Li and Bou-Zeid, 2013), the influence of changeable weather conditions (i.e., precipitation events, cloudy conditions) was minimized and thus the errors may be smaller compared to studies analyzing an entire summer. Another reason might be the number and level of detail of the spatial variables used in this study.

The models include variables from different categories such as land cover, topography as well as vegetation parameters. The construction parameters buildings (LC_B) and sealed areas (OS_SE) resulted as important warming factors. Such construction features are key variables for nighttime UHI intensities (Oke et al., 2017) and were also reported by other studies, while the exact parametrization of the variables used vary (Ivajnšič et al., 2014; Zhou et al., 2014; Theeuwes et al., 2017; Shi et al., 2018; Wicki et al., 2018).

On the other hand, water bodies (OS_WA) turned out as an important cooling factor during night. As the Aare River is the dominant water feature in the city of Bern, 4 out of 7 stations with more than 1% water within the buffer were located relatively close to the river. However, the other three stations also show below average UHI intensities. These stations are located next to a little lake, a little stream, or an outdoor swimming pool indicating that adaptation plans concerning "blue measures" (e.g., restoring of the city streams back to the surface) may have a cooling effect on nighttime temperatures. However, the buffer radius and thus the spatial scope of the cooling effect of such blue areas is limited to 150 m in our models. Despite its significant impact on nighttime temperatures found here, such blue areas as cooling factors have not been found in previous studies. They were either not incorporated (Theeuwes et al., 2017) or their influence on nighttime UHI intensities remained insignificant (Shi et al., 2018), or unclear (Steeneveld et al., 2011). In the study of Zhou et al., 2014, an enhanced fraction of open water even led to warmer minimum temperatures. An explanation for these different findings might be the rather low temperatures of the water bodies during summertime in Bern compared to the other study areas, since the way from the Alps, where the Aare river is originating, to Bern is rather short.
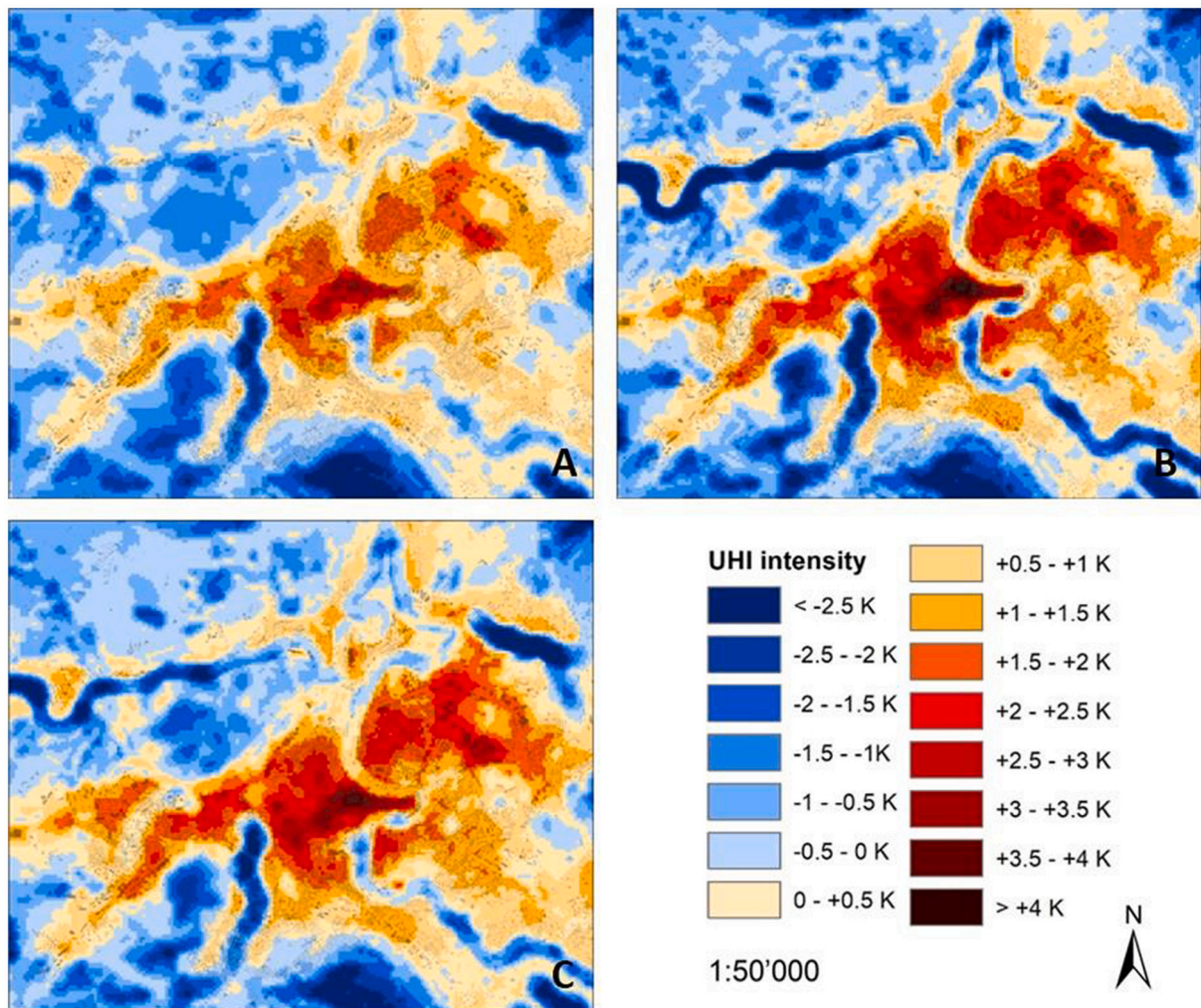
Fig. 5. Resulting spatial patterns of the UHI during HW18 (A), HW19.1 (B) and HW19.2 (C).

In most studies, cooling factors regarding nocturnal UHI intensities are often related to vegetation or green areas. Theeuwes et al. (2017) included the fractional vegetation cover in a 500 m radius in their model and Steeneveld et al. (2011) investigated the influence of urban green vegetation within a 600 m radius. In both studies, the vegetation showed a significant cooling effect on the daily maximum UHI occurring during nighttime. The variable "fractional vegetation cover" with a radius of 400 m was also a significant predictor in two out of five nighttime LUR models by Shi et al. (2018) and the variable "high ratio of green area" is the most important cooling variable during nighttime in the study of Chen et al. (2019). With regard to our study, there is a significant cooling sign during daytime (supplementary material), but the interpretation of the effect of vegetation parameters during nighttime is not straight forward. While higher numbers of trees (AMT) showed a cooling effect, vegetation height (VH) was positively correlated with UHI intensity (Table 4). Single trees in the city are mostly found in open spaces with pervious land cover (i.e., parks or cemeteries), which likely have a cooling effect through enhanced evapotranspiration and open horizons. In forests however, the vegetation is markedly higher and although forested areas consist of unsealed surfaces, temperatures are not markedly lower during nighttime. This finding might be explained by its blocking effect on local wind circulation patterns or by the limiting influence of a dense canopy layer on outgoing longwave radiation (Oke et al., 2017).

Finally, the variable flow accumulation (FLAC) which was used as a proxy for cold air drainage by topography and acts as a significant cooling factor during nighttime (Table 4), has not been included in similar studies. This may be due to the absence of topographical heterogeneity across the investigated study areas (Zhou et al., 2014), the coarser measurement network (Shi et al., 2018), or the difficulty to map such cold air flows (Wicki et al., 2018). In Bern, such cold air channels likely play an important role due to its complex topography (Bigg et al., 2014). Although acknowledging the strong simplification applied here by ignoring potential dependences on wind direction, wind shear, as well as regional scale cold air flows from the Alps (Mathys et al., 1980), this variable has been used to estimate topography-related cold air drainage potential in ecological studies (i.e., Chung et al., 2006; Ashcroft and Gollan, 2012) and can be calculated with a relatively low amount of computational resources from DEMs. However, the application of FLAC in
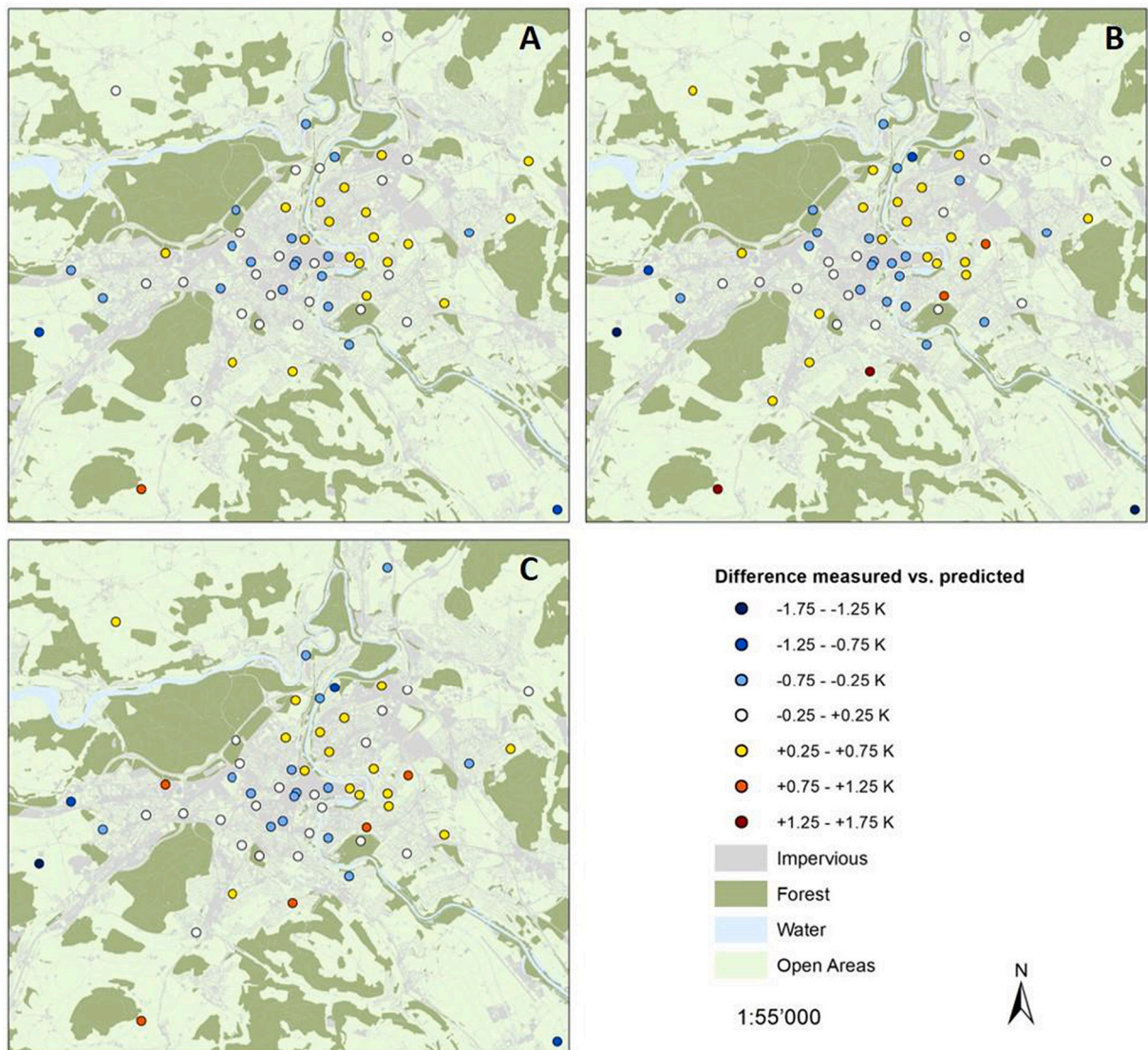
Fig. 6. Difference between the measured and the modelled UHI intensities during HW18 (A), HW19.1 (B) and HW19.2 (C).

an urban environment is a new approach and since the buildings are ignored for that variable, the calculated flows might rather show potential than effective cooling paths.

4.1.2. Differences between heatwaves

The comparison of regression coefficients between the different heatwaves reveals stronger positive and negative coefficients during HW19.1, and weaker coefficients during HW18 (Table 4). This is in line with the higher mean T_{avg} values of HW19.1 (Table 2) and larger UHI intensities observed during that heatwave (Fig. 3), which explains the slight differences of the variables LC_B, OS_SE, FLAC, and AMT between the heatwaves. The increase in regression coefficients of vegetation height (VH) and water bodies (OS_WA) from HW18 to HW19.1 is substantial and is not likely to be only triggered by higher air temperatures. Regarding vegetation height, a possible explanation might be that summer 2018 was extraordinary dry (MeteoSwiss, 2019). The canopy layer could have been less dense during HW18, leading to a reduced blocking of the outgoing longwave radiation and of the wind flows. The three forest-stations in the measurement network support this hypothesis, having negative UHI intensities during HW18 (−0.32 K), but slightly positive UHI intensities during HW19.1 and HW19.2 (0.06 K and 0.23 K). Regarding the water bodies, data of the Federal Office for the environment (BAFU, 2020) showed that mean nocturnal water temperature of the Aare River was lowest during HW19.1 (17.5 °C), moderate during HW19.2 (19.9 °C) and highest during HW18 (21.7 °C). This may explain the enhanced cooling effect of OS_WA during HW19.1 and HW19.2 in the model and the larger spread of the UHI in general, since the stations close to the river were related to strongly negative UHI intensities during the heatwaves in 2019.

Comparing the RMSEs of the different models, the same pattern of a higher deviation in HW19.1 is observed (Table 5). According to the validation results, RMSEs of the additional data during HW19.1 and HW19.2 are markedly higher than LOOCV and model RMSEs. This might be explained by the location of the additional measurement stations in 2019, used for this validation step, which were clustered closely around areas of special interest (Fig. 1). Thus, this additional data is far away from being randomly selected.

4.1.3. Quality of UHI maps

The formation of a large-scale UHI during nighttime over the city of Bern is observable on the UHI maps (Fig. 5), with mean nocturnal UHI intensities in the city varying from 1 and 2.5 K during HW18 to 1.5 and 3.5 K during HW19.1 and HW19.2, respectively. This pattern is also reflected in the magnitude and spatial distribution of maximum UHI intensities of up to 3.5 K (HW18), 4 K (HW19.2), and 4.5 K (HW19.1) occurring in the upper city center. These mean and max UHI intensities are in line with point observations from different cities in Switzerland (Gehrig et al., 2018) where the mean values of 12 out of 16 stations lay between 1 and 3 K and the 95% percentile of 11 out of 16 between 3 and 5 K. Waterbodies as well as the topography are the most important cooling features in those maps (Fig. 5). The cooling of the water bodies is much stronger in HW19.1 and HW19.2 compared to HW18. The Aare river is even dividing the UHI in a western and an eastern part which gives the UHI of Bern a special shape with two hotspots. The spatial dispersion of the cool areas originating from water bodies is however limited to the buffer radius of 150 m (Table 3). The cooling of the topography variable "flow accumulation" is similar throughout all heatwaves. Four strong cold air drainage channels are visible on the nighttime maps which enter directly into the residential areas with a gradient of up to 5 K in the valleys "Köniztal" and "Worblental" compared to its surroundings. Unfortunately, there is no LCD directly located in those channels, which makes a verification of the rather unlikely magnitude of the cooling of those topographic features in this study impossible. Since buildings are ignored by the variable, especially the cooling channel in the southwest, which enters into the built-up area, is questionable and must be interpreted with caution. More research is needed in order to evaluate the possibilities of the use of cold air drainage proxies such as FLAC in cities with complex terrain. To sum up, cold air accumulation seems to have an important influence on the nighttime air temperature variability, but the exact features (intensity, intrusion into the built-up areas) remain uncertain.

Regarding the spatial distribution of the differences between modelled and measured UHI intensities (Fig. 6), the largest differences (+/- 1 K) appear in the rural measurement stations outside of the city. The stations in the southeast as well as the station in the west, which show larger differences than 1 K during nighttime are both located in topographic depressions, which might be another indication that these features are still not adequately represented in the model. On the other hand, the UHI intensity of the rural station in the southwest located at a hillslope is underestimated by the model by more than −1 K. Furthermore, it is visible on the map that the air temperature of the eastern parts of the city are rather underestimated and those of the western parts rather overestimated. This means that an additional, not yet included variable might be causing additional warming in the eastern neighborhoods during nighttime. One potential explanation could evolve from complex ventilation regimes of these neighborhoods with not yet captured, smaller scale cold air streams. Such complex ventilation regimes of Bernese neighborhoods were already discussed in the context of air pollution (Mathys et al., 1980). Another hypothesis might be that the included dry adiabatic decrease of 1 K per 100 m (see Section 2.3.2) is too large and that this could have led to the slightly elevated eastern parts of the city being modelled too cold. However, more detailed research regarding the effects of small-scale cold air flows and accumulations on the UHI intensity including buildings, as well as analyses under different synoptic conditions, would be helpful to improve the model performance for our nighttime UHI maps in order to increase their usability for urban planners.

4.2. LUR models in urban planning and design

Based on our results, the use of the LUR method to create a high-resolution UHI map of the city of Bern during heatwaves seems promising. With this method, it is possible to realistically estimate and map small-scale variations in places where no measurement stations are located (Shi et al., 2018). This would not be possible with interpolation methods based on distance functions only, such as simple kriging (Xie et al., 2011). When compared to an existing UHI map of Bern of an average clear summer night at 6 AM derived from a dynamic, process-based urban climate model output (Climate-fit.city project, https://climate-fit.city) the here applied geo-statistical modelling approach has the advantage that various situations (i.e., timespans, times of the day) can be investigated with a relatively low amount of computional resources. However, the spatial extent and variability of the UHI over the city of Bern of the two maps are similar, although the cooling effect of water bodies and cold air accumulation zones seem more pronounced in the geo-statistically derived maps of this study. Furthermore, it should be kept in mind that the LUR models focused on heatwave periods with low variability in the weather patterns, which allowed to exclude these variables from the model parameters. Since it was possible to conduct a robust model for all three heatwaves which likely differed predominantly due to the intensity of the heatwaves, we assume that these models could also be adapted for analyses of UHI intensities during past or future heatwave situations in Bern. If periods including variable synoptic situations (i.e., whole summer) were analyzed, additional meteorological parameters (e.g., wind speed, cloudiness) would have to be incorporated.

The here presented LUR models can be used as a valuable tool for heat adaption strategies for urban planners since the spatial data is publicly available and the data processing rather simple. With the aid of LUR modelling, potential heating or cooling effects of new constructions, planting of trees, or renaturalizations of small city streams on the UHI intensity during a heatwave can be calculated and mapped. In Hongkong, this technique was used to calculate the warming effect (0.5 K) of a construction of a single large building of 20′000 m² on the surrounding neighborhood (Shi et al., 2018). Similar case studies may be conducted with the model presented in this study for heatwave situations in the city of Bern.

Another important novelty of this study is the combination of a low cost measurement approach with publicly available land use

data. Since the geospatial datasets used in this study are available for the entire country and the data processing in GIS is rather simple, LUR models and resulting UHI maps could be developed for any city in Switzerland at relatively low costs. However, the direct application of the here presented models to other cities is rather limited due to the importance of local features in Bern such as the Aare river, the complex topography or the location of the city at the boundary between mountainous and rather plain landscape. At least some local measurement stations would be needed in a city to adjust the models to the local environment and validate them. If we broadening the potential scope to Europe or even the world, the development and availability of high-quality land use datasets may be another restriction and should therefore be fostered in regions worldwide. An interesting approach could include the generation of spatial variables based on global datasets in order to make this method more attractive for cities worldwide. One potential framework to plan and organize such an urban database is the ongoing WUDAPT (World Urban Database and Portal Tool) project (Ching et al., 2018), which aims at providing local climate zone classifications (Stewart and Oke, 2012) for numerous cities on a global scale.

However, several limitations of the LUR modelling approach are worthwhile to be mentioned. First, the performance of the LUR model depends to a large degree on the quality and the quantity of the temperature data used. Thus, potential biases of the temperature measurement devices need to be adequately incorporated. As described by Gubler et al. (2021), daytime biases of the LCD data used here are quite substantial, which makes an interpretation of those models and maps subject to uncertainty (see supplementary material). The development of improved LCDs with an integrated ventilation system would thus be an important step to enhance the reliability of daytime UHI models. Another improvement would be to include humidity sensors. Additional data on humidity would enrich studies on urban heat and heat stress with another relevant variable besides temperature, and apparent temperature (e.g., Schatz and Kucharik, 2015) or even thermal comfort indices could be modelled and mapped (e.g., Morabito et al., 2014). The development of advanced sensors with the aim of remaining "low cost" is thus one of the major challenges for the improvement and the extension of similar studies. Second, regarding the predictor variables, important meteorological parameters such as cloudiness, windspeed, local wind systems, or precipitation are not included in the present study, which was possible since meteorologically homogeneous periods were analyzed. As a consequence, the incorporation of these parameters would be needed to compare heatwaves with other synoptic situations. In sum, further research and case studies for cities with complex topography in differing climatic contexts would enrich the potential of the LUR approach in modelling UHI intensities and further applications related to it.

5. Conclusions

The aim of this study was to apply and evaluate the LUR approach for modelling UHI intensities in a city with complex terrain during three heatwaves. Based on air temperature data from a dense network of low cost measurement devices and 14 GIS-derived, publicly available spatial variables, we calculated and mapped the spatial pattern of the UHI intensity and investigated the effect of single predictor variables. Despite the restriction of using the same variables during heatwaves in order to get a statistically and theoretically robust model, a good performance of the nighttime models (R^2 0.77–0.80) was achieved. The most important warming variables used in the models were related to human-made constructions, whereas blue and green variables and topographical features were used as cooling factors.

The LUR approach made it possible to spatially interpolate the point-based data of the 60 measurement locations in a much more meaningful way than using other simple distance-based geostatistical interpolation approaches (i.e., kriging). The combination of a low cost network with a resource efficient and straightforward data processing method is thus very promising. However, more research on the parametrization of topographical features (i.e., cold air accumulation) as well as the inclusion of meteorological parameters is needed in order to improve the developed LUR models in cities with complex terrain and to expand the time period from a heatwave situation to a whole summer season with variable synoptic patterns.

Data availability

The raw data used for the analysis is available via the supplementary material. High-resolution maps of the spatial pattern of the nocturnal UHI during the heatwave periods can be accessed and downloaded from: https://boris.unibe.ch/id/eprint/154903

Funding

Author contributions

MB led the conceptualization of the study, managed the data curation, wrote the original draft, revised and edited it and led the measurement campaign in 2019. MG initiated the measurement network, led the measurement campaign in 2018 and contributed to the conceptualization and the methodology. AH contributed to the software design. SB contributed to the conceptualization and supervised the research project. MG, SB and AH commented on and refined all versions of the manuscript.

Declaration of Competing Interest

The authors declare that they have no known competing financial interests or personal relationships that could have appeared to influence the work reported in this paper.

Acknowledgements

Appendix A. Supplementary data

Supplementary data to this article can be found online at https://doi.org/10.1016/j.uclim.2021.100885.

References

Ashcroft, M.B., Gollan, J.R., 2012. Fine-resolution (25 m) topoclimatic grids of near-surface (5 cm) extreme temperatures and humidities across various habitats in a large (200× 300 km) and diverse region. Int. J. Climatol. 32 (14), 2134–2148.

AVR – Amtliche Vermessung Reduziert (EN: "Reduced Cadastral Survey"), 2019. Amt für Geoinformation des Kantons Bern – Office for Geoinformation of the Canton of Bern.

BAFU, 2020. 10-Minuten-Mittel Wassertemperaturen der Station 2135, Bern-Schönau vom 01.05.2018–30.09.2019 (EN: "10-minutes mean water temperatures at station 2135, Bern-Schönau from 01.05.2018 to 30.09.2019"). Received on the 19.02.2020 via mail.

BAFU (Hrsg.), 2016. Hitze und Trockenheit im Sommer 2015. Auswirkungen auf Mensch und Umwelt (EN: "Heat and drought during summer 2015. Effects on people and the environment"). Bundesamt für Umwelt BAFU – Federal Office for the Environment FOEN, Bern. Umwelt-Zustand Nr. 1629: 108 S.

BAFU et al. (Hrsg.), 2019. Hitze und Trockenheit im Sommer 2018. Auswirkungen auf Mensch und Umwelt (EN: "Heat and drought during summer 2018. Effects on people and the environment"). Bundesamt für Umwelt BAFU – Federal Office for the Environment FOEN, Bern. Umwelt-Zustand Nr. 1909: 96 S.

BFS (Bundesamt für Statistik), 2015. Szenarien zur Bevölkerungsentwicklung der Schweiz, 2015–2045 (EN: "Scenarios on the development of the population of Switzerland 2015 to 2045"). Bundesamt für Statistik (BFS) – Federal Statistical Office, Neuenburg. Bevölkerung / Bildung und Wissenschaft. BFS- Nummer 201–1501.

BFS (Bundesamt für Statistik), 2019. Statistik der Schweizer Städte 2019, Wohnbevölkerung (EN:"Swiss cities statistics 2019, resident population"). URL: https://www.bfs.admin.ch/bfs/de/home/statistiken/kataloge-datenbanken/tabellen.assetdetail.8046577.html (last access: 06/04/2021).

Bigg, G.R., Wise, S.M., Hanna, E., Mansell, D., Bryant, R.G., Howard, A., 2014. Synoptic climatology of cold air drainage in the Derwent Valley, Peak District, UK. Meteorol. Appl. 21 (2), 161–170.

CH2018, 2018. CH2018 – Climate Scenarios for Switzerland. Technical Report. National Centre for Climate Services, Zurich, 271 pp.

Chapman, L., Muller, C.L., Young, D.T., Warren, E.L., Grimmond, C.S.B., Cai, X.M., Ferranti, E.J., 2015. The Birmingham urban climate laboratory: an open meteorological test bed and challenges of the smart city. Bull. Am. Meteorol. Soc. 96 (9), 1545–1560.

Chen, Y.C., Liao, Y.J., Yao, C.K., Honjo, T., Wang, C.K., Lin, T.P., 2019. The application of a high-density street-level air temperature observation network (HiSAN): the relationship between air temperature, urban development, and geographic features. Sci. Total Environ. 685, 710–722.

Ching, J., Mills, G., Bechtel, B., See, L., Feddema, J., Wang, X., Ren, C., Brousse, O., Martilli, A., Neophytou, M., Mouzourides, P., Stewart, I., Hanna, A., Ng, E., Foley, M., Alexander, P., Aliaga, D., Niyogi, D., Shreevastava, A., Bhalachandra, P., Masson, V., Hidalgo, J., Fung, J., Andrade, M., Baklanov, A., Dai, W., Milcinski, G., Demuzere, M., Brunsell, N., Pesaresi, M., Miao, S., Mu, Q., Chen, F., Theeuwes, N., 2018. WUDAPT: an urban weather, climate, and environmental modeling infrastructure for the anthropocene. Bull. Am. Meteorol. Soc. 99 (9), 1907–1924.

Chung, U., Seo, H.H., Hwang, K.H., Hwang, B.S., Choi, J., Lee, J.T., Yun, J.I., 2006. Minimum temperature mapping over complex terrain by estimating cold air accumulation potential. Agric. For. Meteorol. 137 (1–2), 15–24.

Crowther, T.W., Glick, H.B., Covey, K.R., Bettigole, C., Maynard, D.S., Thomas, S.M., Smith, J.R., Hintler, G., Duguid, M.C., Amatulli, G., Tuanmu, M.-N., Jetz, W., Salas, C., Stam, C., Piotto, D., Tavani, R., Green, S., Bruce, G., Williams, S.J., Wiser, S.K., Huber, M.O., Hengeveld, G.M., Nabuurs, G.-J., Tikhonova, E., Borchardt, P., Li, C.-F., Powrie, L.W., Fischer, M., Hemp, A., Homeier, J., Cho, P., Vibrans, A.C., Umunay, P.M., Piao, S.L., Rowe, C.W., Ashton, M.S., Crane, P.R., Bradford, M.A., 2015. Mapping tree density at a global scale. Nature 525 (7568), 201–205.

Deilami, K., Kamruzzaman, M., Liu, Y., 2018. Urban heat island effect: a systematic review of spatio-temporal factors, data, methods, and mitigation measures. Int. J. Appl. Earth Obs. Geoinf. 67, 30–42.

Development Team, Q.G.I.S., 2018. QGIS Geographic Information System. Open Source Geospatial Foundation Project. http://qgis.osgeo.org.

EEA (European Environment Agency), 2017. Climate change, impacts and vulnerability in Europe 2016 An indicator-based report, Luxembourg, 424 pp. ISBN 978-92-9213-835-6.

ESRI, 2016. ArcGIS. Version 10.4. Release Date May 31, 2016.

Gehrig, R., König, N., Scherrer, S., 2018. Städtische Wärmeinsel in der Schweiz - Klimatologische Studie mit Messdaten in fünf Städten (EN: "Urban heat islands in Switzerland – climatological study with measurement data in five cities"). Fachber. MeteoSchweiz – MeteoSwiss technical report 273, 61 pp.

Ginzler, C., Hobi, M.L., 2015. Countrywide stereo-image matching for updating digital surface models in the framework of the Swiss National Forest Inventory. Remote Sens. 7 (4), 4343–4370.

Grize, L., Huss, A., Thommen, O., Schindler, C., Braun-Fahrländer, C., 2005. Heat wave 2003 and mortality in Switzerland. In: Swiss Medical Weekly 135(13–14): S. 200–205. MeteoSchweiz 2019: Klimabulletin Jahr 2018. Zürich.

Gubler, M., Christen, A., Remund, J., Brönnimann, S., 2021. Evaluation and Application of a Low Cost Measurement Network to Study Intraurban Temperature Differences during Record Summer 2018 (In press).

Hoek, G., Beelen, R., De Hoogh, K., Vienneau, D., Gulliver, J., Fischer, P., Briggs, D., 2008. A review of land-use regression models to assess spatial variation of outdoor air pollution. Atmos. Environ. 42 (33), 7561–7578.

IPCC, 2014. Climate Change 2014: Synthesis Report. Contribution of Working Groups I, II and III to the Fifth Assessment Report of the Intergovernmental Panel on Climate Change [Core Writing Team, R.K. Pachauri and L.A. Meyer (eds.)]. IPCC, Geneva, Switzerland, 151 pp.

Ivajnšič, D., Kaligarič, M., Žiberna, I., 2014. Geographically weighted regression of the urban heat island of a small city. Appl. Geogr. 53, 341–353.

James, G., Witten, D., Hastie, T., Tibshirani, R., 2013. An Introduction to Statistical Learning, 112. Springer, New York, pp. 3–7.

Jerrett, M., Arain, A., Kanaroglou, P., Beckerman, B., Potoglou, D., Sahsuvaroglu, T., Morrison, J., Giovis, C., 2005. A review and evaluation of intraurban air pollution exposure models. J. Expo. Sci. Environ. Epidemiol. 15 (2), 185–204.

Kato, S., Yamaguchi, Y., 2007. Estimation of storage heat flux in an urban area using ASTER data. Remote Sens. Environ. 110 (1), 1–17.

Köllner, P., Gross, C., Schäppi, B., Füssler, J., Lerch, J., Nauser, M., 2017. Klimabedingte Risiken und Chancen. Eine schweizweite Synthese. (EN: "Climate-related risks and opportunities. A Switzerland-wide synthesis."). Bundesamt für Umwelt (BAFU) – Federal Office for the Environment (FOEN), Bern. Umwelt-Wissen Nr. 1706: 148 S.

Konarska, J., Lindberg, F., Larsson, A., Thorsson, S., Holmer, B., 2014. Transmissivity of solar radiation through crowns of single urban trees - application for outdoor thermal comfort modelling. Theor. Appl. Climatol. 117 (3–4), 363–376.

Kottek, M., Grieser, J., Beck, C., Rudolf, B., Rubel, F., 2006. World map of the Köppen-Geiger climate classification updated. Meteorol. Z. 15 (3), 259–263.

Li, D., Bou-Zeid, E., 2013. Synergistic interactions between urban heat islands and heat waves: the impact in cities is larger than the sum of its parts. J. Appl. Meteorol. Climatol. 52 (9), 2051–2064.

Lindberg, F., Grimmond, C.S.B., Gabey, A., Huang, B., Kent, C.W., Sun, T., Theeuwes, N.E., Järvi, L., Ward, H.C., Capel-Timms, I., Chang, Y., Jonsson, P., Krave, N., Liu, D., Meyer, D., Olofson, K.F.G., Tan, J., Wästberg, D., Xue, L., Zhang, Z., 2018. Urban multi-scale environmental predictor (UMEP): an integrated tool for city-based climate services. Environ. Model. Softw. 99, 70–87.

Mathys, H., Maurer, R., Messerli, B., Wanner, H., Winiger, M., 1980. Klima und Lufthygiene im Raum Bern. Resultate des Forschungsprogrammes KLIMUS und ihre Anwendung in der Raumplanung. (EN: "Climate and air pollution control in the area of Bern. Results of the KLIMUS research program and the application in urban planning") Schweizerische Naturfroschende Gesellschaft (7), 40 S., Bern.

Meehl, G.A., Tebaldi, C., 2004. More intense, more frequent, and longer lasting heat waves in the 21st century. Science 305 (5686), 994–997.

Meier, F., Fenner, D., Grassmann, T., Otto, M., Scherer, D., 2017. Crowdsourcing air temperature from citizen weather stations for urban climate research. Urban Clim. 19, 170–191.

MeteoSwiss, 2018. Klimanormwerte Bern/Zollikofen, Normperiode 1981–2010. (EN: "Climate Normals Bern/Zollikofen, Normperiod 1981–2010"). Federal Office of Meteorology and Climatology, Zurich.

MeteoSwiss, 2019. Klimabulletin Jahr 2018 (EN: "Climate Report Year 2018"). Federal Office of Meteorology and Climatology Zürich.

MeteoSwiss, 2020. Klimabulletin Jahr 2019 (EN: "Climate Report Year 2019"). Federal Office of Meteorology and Climatology Zürich.

Morabito, M., Crisci, A., Messeri, A., Capecchi, V., Modesti, P.A., Gensini, G.F., Orlandini, S., 2014. Environmental temperature and thermal indices: what is the most effective predictor of heat-related mortality in different geographical contexts? Sci. World J. 2014, 15. https://doi.org/10.1155/2014/961750. Article ID 961750.

Morris, C.J.G., Simmonds, I., Plummer, N., 2001. Quantification of the influences of wind and cloud on the nocturnal urban heat island of a large city. J. Appl. Meteorol. 40 (2), 169–182.

Muller, C.L., Chapman, L., Grimmond, C.S.B., Young, D.T., Cai, X., 2013. Sensors and the city: a review of urban meteorological networks. Int. J. Climatol. 33 (7), 1585–1600.

Oke, T.R., 1995. The heat island of the urban boundary layer: characteristics, causes and effects. In: Cermak, J.E., Davenport, A.G., Plate, E.J., Viegas, D.X. (Eds.), Wind Climate in Cities. Kluwer Academic, pp. 81–102.

Oke, T.R., Mills, G., Christen, A., Voogt, J.A., 2017. Urban Climates. Cambridge University Press, Bundesamt für Umwelt (BAFU) – Federal Office for the Environment (FOEN), Bern. Umwelt-Wissen Nr. 1706: 148 S.

Perkins, S.E., 2015. A review on the scientific understanding of heatwaves—their measurement, driving mechanisms, and changes at the global scale. Atmos. Res. 164, 242–267.

R Development Core Team, 2008. R: A Language and Environment for Statistical Computing. R Foundation for Statistical Computing, Vienna, Austria. ISBN 3-900051-07-0, URL. http://www.R-project.org.

Robine, J.M., Cheung, S.L., Le Roy, S., van Oyen, H., Herrmann, F.R., 2007. Report on excess mortality in europe during summer 2003. In: EU Community Action Programme for Public Health, Grant Agreement 2005114, 15 S.

Salvato, J.A., Nemerow, N.L., Agardy, F.J., 2003. Environmental Engineering. John Wiley & Sons.

Schatz, J., Kucharik, C.J., 2015. Urban climate effects on extreme temperatures in Madison, Wisconsin, USA. Environ. Res. Lett. 10 (9), 094024.

Shi, Y., Katzschner, L., Ng, E., 2018. Modelling the fine-scale spatiotemporal pattern of urban heat island effect using land use regression approach in a megacity. Sci. Total Environ. 618, 891–904.

Steeneveld, G.J., Koopmans, S., Heusinkveld, B.G., Van Hove, L.W.A., Holtslag, A.A.M., 2011. Quantifying urban heat island effects and human comfort for cities of variable size and urban morphology in the Netherlands. J. Geophys. Res. Atmos. 116 (D20).

Stewart, I.D., 2011. A systematic review and scientific critique of methodology in modern urban heat island literature. Int. J. Climatol. 31 (2), 200–217.

Stewart, I.D., Oke, T.R., 2012. Local climate zones for urban temperature studies. Bull. Am. Meteorol. Soc. 93 (12), 1879–1900.

Szymanowski, M., Kryza, M., 2009. GIS-based techniques for urban heat island spatialization. Clim. Res. 38 (2), 171–187.

Theeuwes, N.E., Steeneveld, G.J., Ronda, R.J., Heusinkveld, B.G., Van Hove, L.W.A., Holtslag, A.A.M., 2014. Seasonal dependence of the urban heat island on the street canyon aspect ratio. Q. J. R. Meteorol. Soc. 140 (684), 2197–2210.

Theeuwes, N.E., Steeneveld, G.J., Ronda, R.J., Holtslag, A.A., 2017. A diagnostic equation for the daily maximum urban heat island effect for cities in northwestern Europe. Int. J. Climatol. 37 (1), 443–454.

United Nations, Department of Economic and Social Affairs, Population Division, 2019. World Urbanization Prospects: The 2018 Revision (ST/ESA/SER.A/420). United Nations, New York.

Wanner, H., Hertig, J.A., 1984. Studies of urban climates and air pollution in Switzerland. J. Clim. Appl. Meteorol. 23 (12), 1614–1625.

Wicki, A., Parlow, E., Feigenwinter, C., 2018. Evaluation and modeling of urban heat island intensity in Basel, Switzerland. Climate 6 (3), 55.

Xie, D., Liu, Y., Chen, J., 2011. Mapping urban environmental noise: a land use regression method. Environ. Sci. Technol. 45 (17), 7358–7364.

Zhou, W., Ji, S., Chen, T.H., Hou, Y., Zhang, K., 2014. The 2011 heat wave in Greater Houston: effects of land use on temperature. Environ. Res. 135, 81–87.